Article

Cell Metabolism

A Systems Approach to Reverse Engineer Lifespan Extension by Dietary Restriction

Graphical Abstract

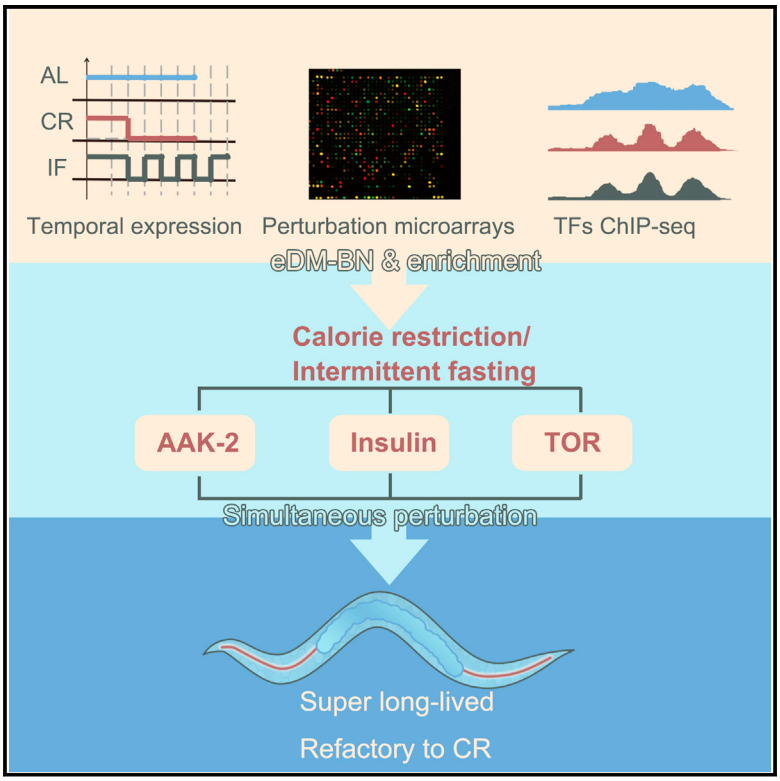

Authors

Lei Hou, Dan Wang, Di Chen, ..., Joseph McDermott, William B. Mair, Jing-Dong J. Han

Correspondence

jdhan@picb.ac.cn

In Brief

Hou et al. used unbiased systems approaches to identify novel regulatory networks for dietary restriction in *C. elegans*. They uncover three transcriptomic modules, which, when simultaneously targeted, result in extremely long-lived animals refractory to dietary restriction. This innovative reverse engineering approach highlights the extensive feedback controls underlying aging.

Highlights

- We obtain temporally resolved effects of diet restriction on aging transcriptomes
- Early responses involve metabolism; late involve cell cycle and DNA damage
- We find three regulator groups with novel regulators separated by target specificity
- Regulator feedbacks are leveraged to fully recapitulate diet restriction effects

Accession Numbers

GSE77111

Hou et al., 2016, Cell Metabolism *23*, 529–540
March 8, 2016
http://dx.doi.org/10.1016/j.cmet.2016.02.002

CellPress

Cell Metabolism
Article

A Systems Approach to Reverse Engineer Lifespan Extension by Dietary Restriction

Lei Hou,[1,6] Dan Wang,[1,2,6] Di Chen,[3,6] Yi Liu,[1,4] Yue Zhang,[5] Hao Cheng,[1,2] Chi Xu,[1,2] Na Sun,[1] Joseph McDermott,[1] William B. Mair,[5] and Jing-Dong J. Han[1,*]
[1]Key Laboratory of Computational Biology, CAS Center for Excellence in Molecular Cell Science, Collaborative Innovation Center for Genetics and Developmental Biology, Chinese Academy of Sciences-Max Planck Partner Institute for Computational Biology, Shanghai Institutes for Biological Sciences, Chinese Academy of Sciences, 320 Yue Yang Road, Shanghai 200031, China
[2]Graduate University of Chinese Academy of Sciences, Beijing 100049, China
[3]State Key Laboratory of Pharmaceutical Biotechnology and MOE Key Laboratory of Model Animals for Disease Study, Model Animal Research Center, Nanjing University, Nanjing, Jiangsu 210061, China
[4]Beijing Key Lab of Traffic Data Analysis and Mining, School of Computer and Information Technology, Beijing Jiaotong University, Beijing 100044, China
[5]Harvard T.H. Chan School of Public Health, Boston, MA 02115, USA
[6]Co-first author
*Correspondence: jdhan@picb.ac.cn
http://dx.doi.org/10.1016/j.cmet.2016.02.002

SUMMARY

Dietary restriction (DR) is the most powerful natural means to extend lifespan. Although several genes can mediate responses to alternate DR regimens, no single genetic intervention has recapitulated the full effects of DR, and no unified system is known for different DR regimens. Here we obtain temporally resolved transcriptomes during calorie restriction and intermittent fasting in *Caenorhabditis elegans* and find that early and late responses involve metabolism and cell cycle/DNA damage, respectively. We uncover three network modules of DR regulators by their target specificity. By genetic manipulations of nodes representing discrete modules, we induce transcriptomes that progressively resemble DR as multiple nodes are perturbed. Targeting all three nodes simultaneously results in extremely long-lived animals that are refractory to DR. These results and dynamic simulations demonstrate that extensive feedback controls among regulators may be leveraged to drive the regulatory circuitry to a younger steady state, recapitulating the full effect of DR.

INTRODUCTION

Dietary restriction (DR) induces lifespan extension in yeast, worms, flies, mice, and monkeys (Fontana et al., 2010; Kenyon, 2010). Several key signaling pathways and regulators have been identified that partially mediate the effects of DR on aging and lifespan, such as insulin/IGF1-like growth factor signaling pathway, AMPK signaling pathway, TOR signaling pathway, and the sirtuin protein family (Kenyon, 2010). However, none of these pathways are solely responsible for the DR effect, because blocking any of them individually does not fully block DR-induced lifespan extension by all regimens. Thus, although targeting these pathways results in long-lived animals, DR still gives additional benefits. It remains unclear whether different pathways mediate different aspects of DR response, whether they interact with each other in response to DR, or whether they act at different stages of DR.

DR is known to induce systemic changes in a whole organism (Lee et al., 1999; Pletcher et al., 2002; Zhou et al., 2012) and is therefore a good paradigm to learn how regulation of aging can be achieved at the systems level. Previously we compared the midlife liver transcriptome changes induced by caloric restriction or exercise on high-fat- or low-fat-diet mice and identified molecular pathways that correlate with the mean lifespans across different regimens (Zhou et al., 2012). However, transcriptomic analyses of one time point are not sufficient to resolve the cause versus consequence of DR effects, where early starvation signaling must be converted or relayed to late aging regulators to induce long-term health benefits.

Here, using *C. elegans* as a model, we analyzed the temporal profiles of two DR regimens, calorie restriction (CR) and intermittent fasting (IF), to identify early and late gene expression responses to CR and IF, and computationally inferred potential regulators for these responses. We found that early response genes are more significantly changed at the transcriptional level compared to late response genes, and known lifespan regulators tend to display a postreproduction stage reversal of gene expression patterns. Furthermore, we inferred three regulatory modules according to their activity or target profiles: (1) an *rheb-1_let-363/tor* module that targets very early response genes involved in metabolism, (2) an *aak-2_tax-6_xbp-1* module that is rapidly upregulated in response to starvation and represses age-dependent increases in phosphorylation and dephosphorylation processes, and (3) a module containing *daf-16* and *glp-1* and their target transcription factors (TFs) that delay the postreproduction increase in DNA damage response gene expression. Based on these regulatory patterns and the intensive feedback controls between different regulators, we

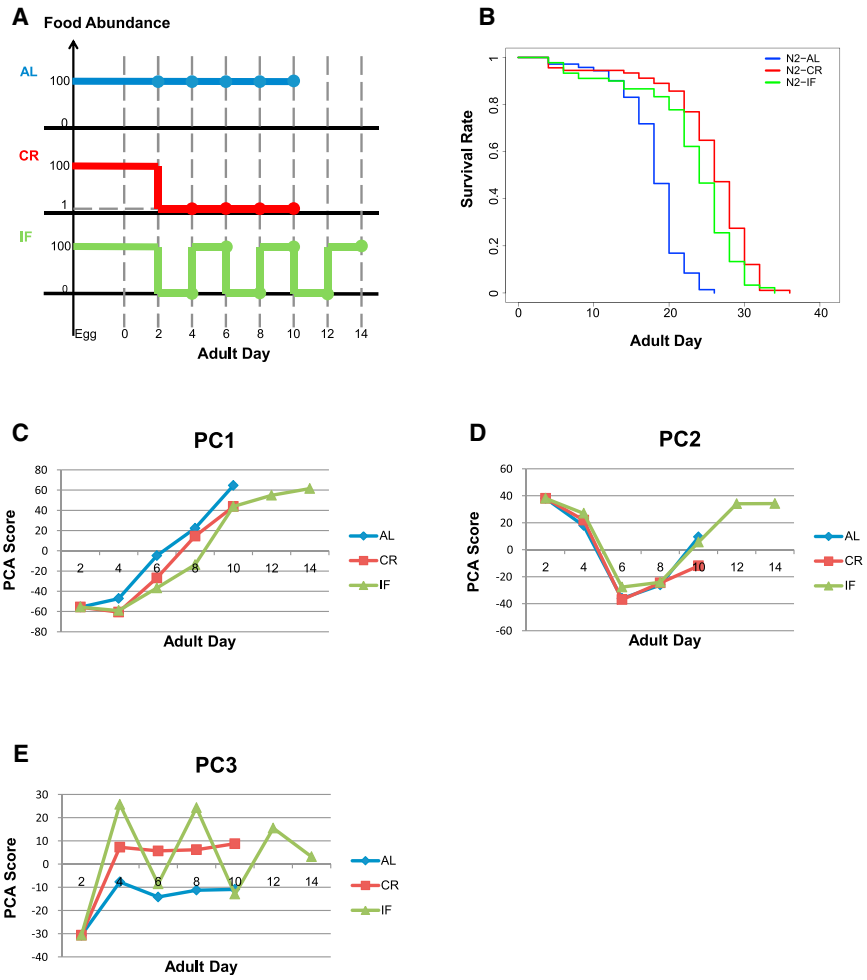

Figure 1. Experimental Design for Temporal Gene Expression Profiles upon CR and IF

(A) All treatments are started on AD 0. Worms are collected on AD 2, 4, 6, 8, and 10 for each condition, and for IF on AD 12 and 14 as well. AL refers to 1×10^{10} bacteria ml^{-1} concentration of OP50 bacteria, CR refers to 1% of AL concentration, and IF refers to 2 days of feeding and 2 days of fasting from AD 0.

(B) Lifespan of N2 worms under AL, CR, and IF conditions.

(C–E) Top three principal components (PCs) in the gene expression data.

Detailed statistics of the lifespan results are presented in Table S4.

computationally predicted that by simultaneously modulating all three regulatory groups, we may be able to leverage the feedback controls to drive the circuitry to a young steady state, and to recapitulate the full transcriptomic changes induced by DR. Supporting this concept, we showed that simultaneous perturbation of all three distinct DR modules results in animals with extreme lifespan extension that is refractory to the effects of DR.

RESULTS

Time Series Analysis of Ad Libitum, CR, and IF Transcriptome

To compare the temporal transcriptome changes during aging under ad libitum (AL), CR, and IF, we started the treatments on adult day (AD) 2 with full dosage of bacteria supplied for worms under AL feeding, 1% dosage for CR, and full dosage of food and fasting provided in turn every 2 days for IF. We collected worms for microarray analysis on AD 2, 4, 6, 8, and 10 for each condition, and an extra two samples on AD 12 and 14 for IF, so that we have three cycles of 2-day feeding and 2-day fasting (Figure 1A). We conducted lifespan assays under these different regimes and found that CR and IF extend the mean lifespan of worms by 40% and 28%, respectively (Figure 1B). The benefit of including a parallel time series of IF experiments to the other time series is 2-fold: first, it facilitates the identification of common responses to both CR and IF; and second, it distinguishes short-term starvation responses from long-term lifespan regulation, as every-2-day feeding and fasting cycles will result in an oscillation pattern for the genes that change in response to starvation. This allowed us to distinguish early gene expression changes from late changes (Figure 1A). Indeed, the first three principal components (PCs) of the gene expression data reflect this. PC1 showed an age-dependent change, delayed by CR and IF (Figure 1C); PC2 a postreproduction day 6–8 reversal pattern (Figure 1D); and PC3 an early response pattern that oscillates with IF starvation-feeding cycles (Figure 1E).

Temporal Expression Patterns Modulated by CR and IF

To objectively detect the detailed expression patterns in the transcriptome data, we applied an adaptive clustering algorithm we recently developed, called Bayesian Information Criterion-Super K means (BIC-SK) algorithm (Zhang et al., 2013). The BIC-SK algorithm automatically detects the optimum number of clusters that best explain the variations in the data and based on this number obtains tight and homogenous clusters using the SK algorithm (Liu et al., 2013). BIC-SK detected 25 gene expression clusters in our transcriptome data (Figure 2A and see Figure S1A and Table S1 available online). They can be mainly described as three large groups: upregulated with age ("Up" group, green branches in Figure 2A), downregulated and then upregulated with age ("Down-Up" group, blue branches), and upregulated and then downregulated with age ("Up-Down" group, red branches). From the majority of the clusters within all three groups, we observed that CR and IF delay aging-related gene expression changes (Figure S1A). These groups of clusters are also well separated by their loadings on the first three PCs (Figure 2B).

Interestingly, the GenAge (Tacutu et al., 2013) annotated lifespan regulators are more enriched in the clusters that display a

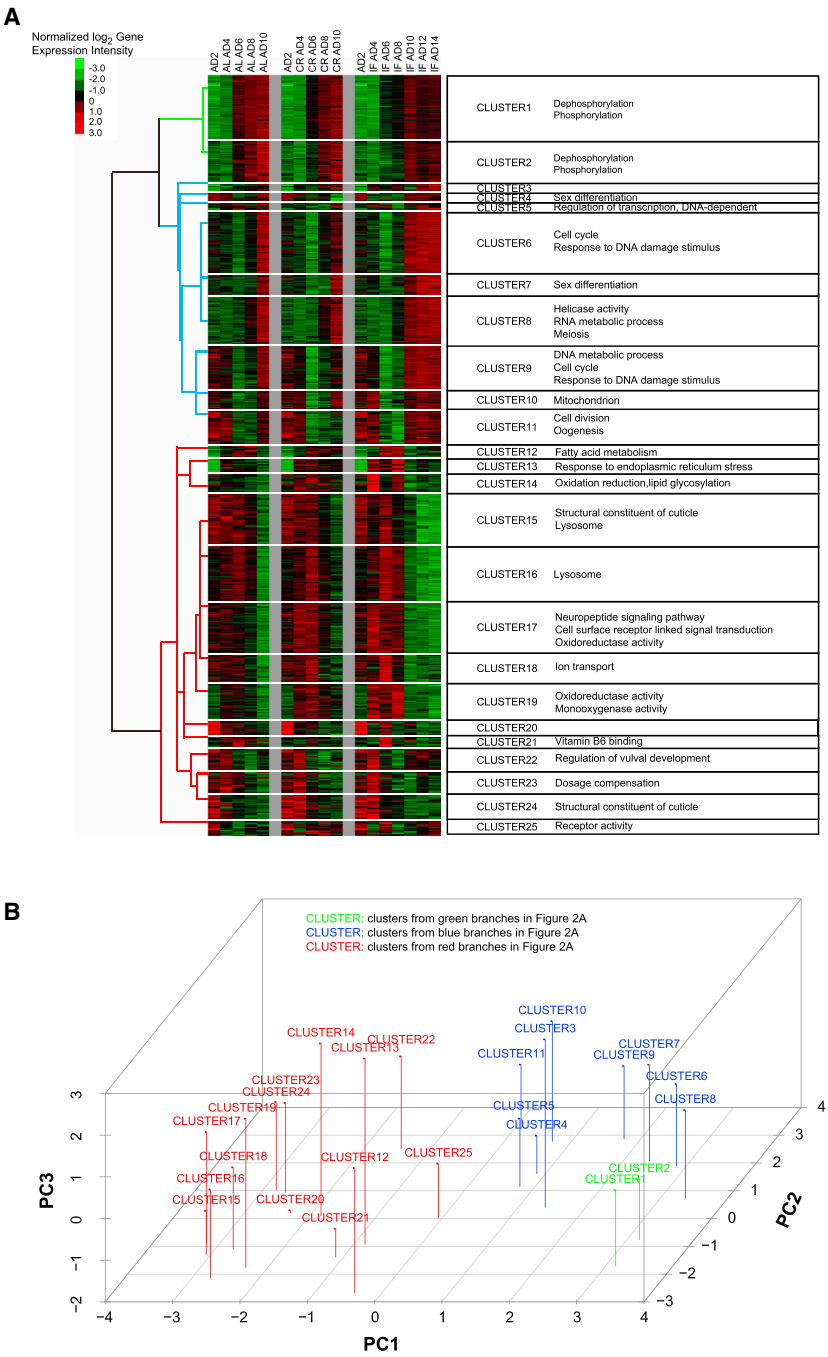

Figure 2. Three Groups of Expression Patterns Modulated by CR and IF or Aging

(A) Genes that show significant change in any sample compared to other samples are clustered using the BIC-SK algorithm, then organized by hierarchical clustering on the BIC-SK cluster centers. The top enriched GO terms are shown for each cluster (Fisher's exact test $p \leq 0.001$). Normalized $\log_2$ transformed expression values are visualized according to the color legend.

(B) Average profiles of each cluster projected onto top three PCs. Red, green, and blue represent clusters in the branches of the same color in Figure 2A, respectively.

See also Figure S1 and Table S1, Table S2, and Table S3.

postreproduction reversal of gene expression patterns (especially clusters 16, 18, and 19 in the "Up-Down" group or 6, 7, and 9 in the "Down-Up" group in Figure 2A) than in those with expression monotonically upregulated with age ("Up" group) (Figure 2A and Table S2; proportion test $p < 0.01$). Moreover, prolongevity regulators are significantly biased for expression patterns like clusters 16, 18, and 19 ("Up-Down" group, and upregulated by CR/IF), while antilongevity regulators are significantly biased for patterns like clusters 6, 7, and 9 ("Down-Up" group, and downregulated by CR/IF) (Fisher exact test, $p = 0.01094$, Table S3), consistent with the prolongevity effect of CR/IF.

To look for the strongest early changes, we focused on patterns that display an obvious and uniform change upon CR and IF compared with AL at the second time point and oscillate with IF treatment. These include clusters 3, 10, 13, 14, 17, 19, 20, 21, and 24, enriched for metabolism-related GO terms, such as Unfolded Protein Response (UPR) and oxidation reduction (Figure S1). Interestingly, most of these early response patterns are in the "Up-Down" group and associate with the genes upregulated by CR and IF, while only two small clusters, 20 and 21, are downregulated. Two other gene clusters, 1 and 2, both belonging to the "Up" group, are downregulated later by CR/IF in life post AD 6, enriched for phosphorylation and dephosphorylation processes. These indicate CR and IF actively and rapidly promote transcription of many genes in response to early-phase starvation, whereas gene expression downregulation by CR/IF might be a secondary downstream effect elicited by the early responses.

Regulators that Potentially Mediate the CR and IF Responses

To infer which genes might mediate the CR and IF responses, we used our recently developed Deletion Mutant Bayesian Network (DM_BN) inference algorithm. DM_BN aims to reverse engineer the regulatory or genetic interactions among various perturbations by comparing the whole genome-wide gene expression changes or differentially expressed genes (DEGs) upon a gene perturbation, e.g., deletion or overexpression of a gene (Li et al., 2013). Unlike the original DM_BN, which we developed to infer regulatory relationships among yeast genetic mutants, here we modified the algorithm to fine-tune the probability inference using real valued data of fold changes rather than discrete data of 1 (upregulated), −1 (downregulated), or 0 (no change) for expression changes, as it is known that aging regulation can be perturbation dosage

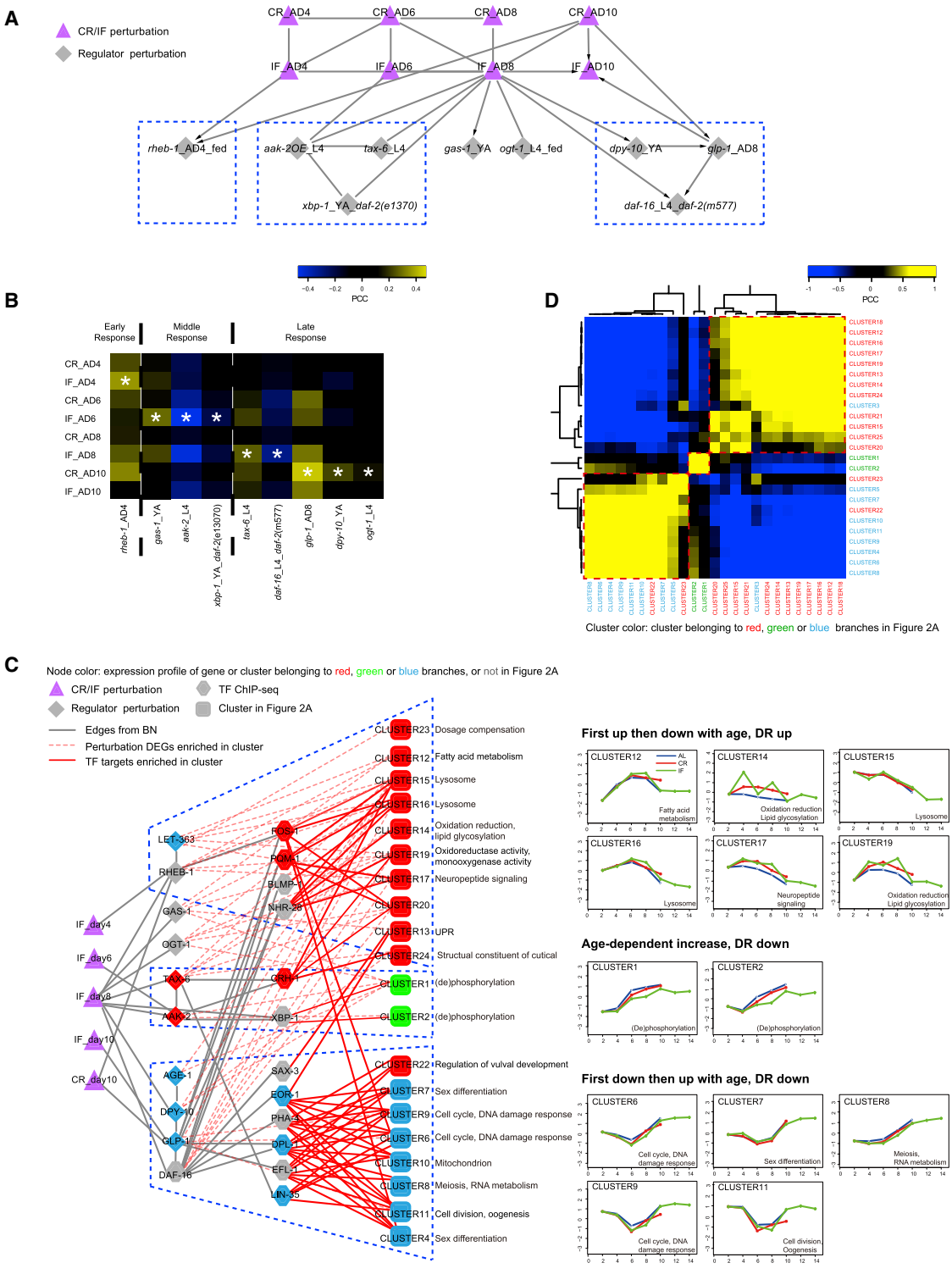

Figure 3. Bayesian Network Inferred Regulators Mediating CR and IF Responses

(A) First-degree neighbors of CR/IF effects on AD 4, 6, 8, and 10 from a genetic network reverse engineered by eDM_BN. CR/IF perturbations and regulator genetic perturbations are shown as triangles and diamonds, respectively. "L4" and "YA" in the node labels stand for larvae 4 and young adult stages, respectively. "*daf-2*(*e1370*)" or "*daf-2*(*m577*)" in the node labels indicates a perturbation is on the background of this mutant.

(B) PCC between DEGs' expression changes from key regulator perturbations (column) and those from CR/IF treatment (row). Genes identified as DEGs (consistent with parameters for eDM_BN, see Supplemental Experimental Procedures) under at least one condition were included in the calculation. Stars mark

(legend continued on next page)

dependent (e.g., strong and weak perturbation on mitochondria function can confer opposite effects on lifespan) (Baruah et al., 2014). We named this algorithm eDM_BN for extended DM_BN (algorithm details are described in the Supplemental Experimental Procedures).

Altogether we collected 73 genetic perturbations versus respective control pairs and treated CR and IF as perturbations. Then we used gene expression fold changes between CR/IF versus AL at each time point and those induced by genetic perturbations to infer an eDM_BN of relationships among the perturbations. eDM_BN inferred genetic perturbations of nine genes directly linked to the CR/IF perturbations at several time points, which indicates that perturbations of these genes closely mimic the CR/IF effects on the transcriptome (Figure 3A). The inferred interactions can be verified by the similarities of gene expression profiles of the DEGs induced by the genetic mutations and by CR/IF (Figure S2). Three cliques appear in the BN, as marked by dashed boxes (Figure 3A). The first consists of *rheb-1*, encoding a small GTPase, connected to nodes IF_AD4 and CR_AD10. The second consists of *aak-2*, encoding the catalytic alpha subunit of AMP-activated protein kinase (AMPK), connected to nodes IF_AD6 and IF_AD8. It also consists of *xbp-1*, a key mediator for ER UPR, and *tax-6*, encoding the homolog of mammalian calcium dependent Ser/Thr phosphatase calcineurin A, connected to IF_AD8 directly and through an *aak-2* connection, respectively. The third clique consists of three genes: *glp-1*, encoding a LIN-12/Notch family receptor, connected to nodes IF_AD10 and CR_AD10; *daf-16*, encoding a forkhead box O (FOXO) TF; and *dpy-10*, encoding a cuticle collagen protein, both connected to the IF_AD8 node (Figure 3A). In addition to the above genes, the IF_AD8 node is also linked to two genes that are known to be involved in lifespan regulation but have not been implicated in DR effect. These are *gas-1*, a lifespan regulator encoding a mitochondria complex I component (Kayser et al., 2004), and *ogt-1*, another lifespan regulator encoding an ortholog of O-linked N-acetylglucosamine (O-GlcNAc) transferase (Rahman et al., 2010). Among the potential regulators above, *rheb-1*, *daf-16*, and *aak-2* have already been implicated in DR (Greer and Brunet, 2009; Greer et al., 2007; Honjoh et al., 2009), while germline activity regulated by *glp-1* and ER UPR regulated by *xbp-1* were reported to be closely related to DR effect (Angelo and Van Gilst, 2009; Chen et al., 2009; Crawford et al., 2007). The roles of *tax-6*, *dpy-10*, *gas-1*, and *ogt-1* genes in DR have not been reported previously, and *gas-1* and *ogt-1* do not belong to the three cliques of regulators, suggesting new pathways mediating the DR effect. From the network, it is also clear that by connecting to the IF_AD4 node, *rheb-1* might be involved in early responses, while the *aak-2* clique is more similar to middle phase changes (AD6 and AD8), and the *daf-16* clique is more similar to late responses. These inferences can be also visually confirmed by the similarity (measured by Pearson Correlation Coefficient [PCC]) of all the DEGs from different perturbations (Figure 3B).

Modular Regulation by Regulators that Potentially Mediate the CR and IF Responses

Next we sought to determine the targets of the predicted regulators to determine whether they regulate all CR/IF-induced changes as a whole or preferentially regulate some changes distinctly and therefore only altogether explain all of the CR/IF-induced changes. To do this, we first extended our eDM_BN to incorporate both genetic perturbation versus control gene expression fold-change data and the TF ChIP-seq data from the modENCODE project (Contrino et al., 2012). This allows expression changes of a TF itself or its targets identified by ChIP-seq to also be included in the analysis to more directly explain the gene expression changes (Experimental Procedures). In this TF-expanded eDM_BN, relationships among the potential regulators and TFs are delineated in a hierarchical layout for visual clarity (Figure 3C). For example, *fos-1*, reported to play a role in IF induced lifespan extension (Uno et al., 2013), based on target profile similarity, is inferred to share targets with *rheb-1* and *glp-1*. This indicates that *fos-1* might be involved in the transcriptional regulation by *rheb-1* and *glp-1*. Additionally, *pqm-1*, reported to play a complementary role to *daf-16* in aging (Tepper et al., 2013), is inferred to share targets with *glp-1* and *daf-16*. Meanwhile, *pha-4*, reported to play an important role in DR-induced lifespan (Panowski et al., 2007), is inferred to share targets with *daf-16*. Using our CoCiter program (Qiao et al., 2013), we found that four other TFs inferred to share targets with DAF-16 (BLMP-1, NHR-28, SAX-3, and EOR-1) are also related to aging or DR (empirical $p = 0.077$) (Figure 3C).

To further explore the modular regulation pattern and the targets of each regulator, we tested each BIC-SK cluster's enrichment for the DEGs induced by the genetic perturbations (versus respective controls) of regulators included in the eDM_BN, and each cluster's enrichment for the targets of each TF by Fisher's exact test (Experimental Procedures). To our surprise, most TF-target relationships and some regulator-target relationships also fall into three domains, or modules, similar to the trimodule structure in Figure 3A. Strikingly, these modules of gene expression clusters, through their regulatory TFs, can be traced to the three regulatory pathways identified by the eDM_BN network, namely the *rheb-1_let-363/tor* pathway, the *aak-2_tax-6_xbp-1* pathway, and the *daf-16_glp-1* pathway (Figure 3C).

the CR/IF treatments with highest similarity (by absolute PCC, $p < 1 \times 10^{-60}$) to each key regulator perturbations, and thus the most likely temporal phase of regulation for each factor.

(C) The regulator-target-cluster network and average gene expression profiles of the clusters. CR/IF perturbations, regulators directly linked to perturbations, TFs, and gene clusters, are represented by triangles, diamonds, hexagons, and squares, respectively. Node color annotations are shown in the graphic legend. A cluster's enrichment for a TF's ChIP-seq targets or a TF genetic perturbation DEG set identified by Fisher's exact test is shown as a red solid edge. A cluster's enrichment for regulator genetic perturbations versus wild-type identified by Fisher's exact test is shown as a red dashed edge. Genetic interactions inferred by eDM_BN are shown as gray edges.

(D) Clustering of target gene clusters based on pairwise PCCs across clusters' GSEA normalized enrichment scores (NES) for differential gene expression under different perturbations. Heatmap color indicates PCC between NES of two different clusters across different perturbation conditions. Color of a cluster label indicates the branch in Figure 2A to which the cluster belongs.

See also Figure S2.

Inside each module, the TFs and regulators share similar target enrichment profiles across different BIC-SK clusters and very similar gene expression patterns, while there is relatively little target-cluster overlap between different modules for these TFs and regulators, or similarity in gene expression patterns (Figure 3C). The *rheb-1_let-363/tor* regulatory module mainly targets clusters 12, 14, 15, 16, 17, 19, and 20, which are enriched for lysosome, oxidation-reduction, lipid glycosylation functions, and neuropeptide signaling pathways (Figure 3C). The genes in these clusters are mostly upregulated by CR/IF and have the largest changes over PC3, the IF oscillation pattern (Figure 2B, Fisher's exact test $p = 7.1 \times 10^{-131}$). The *aak-2_tax-6_xbp-1* module mainly targets the two large clusters, 1 and 2, which have the most significant age-dependent increase (linear regression $R^2 = 0.89$ and 0.88, $p = 0.0167$ and 0.0177 for clusters 1 and 2, respectively) that was delayed by CR/IF, and have the largest changes over PC1 (Figure 2B, Fisher's exact test $p = 1.2 \times 10^{-86}$). The *daf-16_glp-1* module mainly targets clusters 4, 6, 7, 8, 9, 10, and 11, which are enriched for DNA damage response, cell cycle regulation, and mitochondria activities. The genes in these clusters are slightly downregulated by CR/IF (Figure 3C) and have the largest changes over PC2 (Figure 2B, Fisher's exact test $p = 1.0 \times 10^{-316}$). Remarkably, clusters in each module also have similar expression patterns (Figure 3C). These modules of target clusters were also confirmed by clustering based on target enrichment profiles across different perturbations (Figure 3D). Such a trimodule structure of the predicted regulatory network suggests that each of the three pathways can only partially account for the CR/IF effects and that only when modulated together can they simulate the full effect of CR/IF on aging.

Simultaneous Perturbation of Three Modules Simulates CR/IF-Induced Transcriptome Changes

To test the additive effects of the three modules, we simultaneously perturbed the three modules derived from our network analysis (Figure 3C). For the *rheb-1_let-363/tor* regulatory module—since both *rheb-1* and *let-363* mutants are lethal—RSKS-1, the *C. elegans* S6 kinase ortholog acting downstream of RHEB-1 and LET-363/ceTOR, was selected. For the *daf-16_glp-1* module, DAF-2, insulin/IGF receptor in *C. elegans*—the mutant of which promotes lifespan through DAF-16—was selected. For the *aak-2_tax-6_xbp-1* module, *aak-2*—previously reported to mediate the effect of DR—and *tax-6*—which shares downstream targets with *aak-2* (Greer et al., 2007; Mair et al., 2011)—were selected. In the following analyses, *rsks-1(ok1255)*, *daf-2(e1370)*, an *aak-2* overexpression strain (*aak-2(o/e)*), and *tax-6* RNAi were included as genetic perturbations of the selected regulators. We used *tax-6* RNAi because, despite multiple attempts, we failed to obtain a *tax-6*;*daf-2 rsks-1* triple mutant, probably due to embryonic lethality. Previously, double *daf-2 rsks-1* mutants were constructed and reported to extend lifespan to a much greater extent than each single mutant (Chen et al., 2013), which is consistent with our hypothesis that modulating different pathways altogether could lead to longer lifespan. Here, a triple mutant *aak-2(o/e)*;*daf-2 rsks-1* was further constructed by crossing *aak-2(o/e)* and the *daf-2 rsks-1* double mutant to perturb all three modules, and double mutant *daf-2 rsks-1* under *tax-6* RNAi is used as an alternative way to perturb all three modules.

To explore whether perturbing the three modules mimics the CR/IF-induced transcriptome changes, we performed microarray analysis on AD4 worms of wild-type and various single, double, and triple perturbations, including N2, *rsks-1*, *daf-2*, *aak-2(o/e)*, N2 under *tax-6* RNAi, *rsks-1* under *tax-6* RNAi, *daf-2* under *tax-6* RNAi, *daf-2 rsks-1*, *aak-2(o/e)*;*daf-2 rsks-1*, and *daf-2 rsks-1* under *tax-6* RNAi with two replicates for each condition. We chose the AD4 stage for analysis because animals have reached the end of the reproductive period and therefore do not contain many eggs, which may interfere with the gene expression analysis of the whole worm yet are young enough to detect acute effects of interventions/perturbations. We then compared the gene expression ($\log_2$ transformed) fold changes in each sample relative to N2 conditions with those under CR and IF relative to AL on the same day (AD4). To reduce noise from background fluctuations, we focused only on the CR and IF-induced DEGs (Supplemental Experimental Procedures) and calculated the PCCs of these DEGs' fold changes between the genetic and dietary perturbations. The increasing PCCs with the increase in the number of genetic perturbations (Figure 4 for false discovery rate ≤ 0.01; Figure S3 for other cutoffs) indicate that, as more and more modules are genetically perturbed, the transcriptomic changes became more and more similar to those induced by CR/IF.

Perturbing Three Modules Shifts the Network Steady State toward a Longevity State

Why is perturbing three modules more effective than modulating any single module to attain longevity and account for more CR/IF effects? We explored this by computationally simulating the steady-state distributions of the regulatory network under different perturbations. In order to simulate the network dynamics based on the interactions between the three modules, from literature we derived a simplified circuitry consisting of only DAF-2, AAK-2, and RSKS-1 with extensive positive feedback loops to represent the interactions among three modules (Figures 5A and S4A). Using a framework developed by Ma et al. (Ma et al., 2009), we computationally quantified dynamics of the activity of each protein, represented by variables *AAK-2*, *DAF-2*, and *RSKS-1*, respectively. This activity is constrained by total amount of each protein, which is preset to 1 when not perturbed, or preset according to perturbation fold change when perturbed. For example, a perturbation fold change as 2 means the total amount of DAF-2 or RSKS-1 protein is knocked down 2-fold to 1/2 when perturbed by in silico *daf-2* or *rsks-1* mutant, while the total protein for AAK-2 is upregulated 2-fold to 2 when perturbed by *in silico aak-2(o/e)* strain.

We plotted the distribution of the steady states derived from kinetics of the network (when equilibrium is reached for all kinetic equations) over the whole parameter space for wild-type and our different perturbation combinations, including in silico single, double, and triple mutants (Figure 5B). We found that these steady states tend to aggregate at three types of points (red or yellow regions in each plot in Figure 5B): the first corresponds to a young state, where prolongevity AAK-2 is maximally active and antilongevity DAF-2 and RSKS-1 are fully inactive (marked by a purple circle in Figure 5B as an example), while the latter

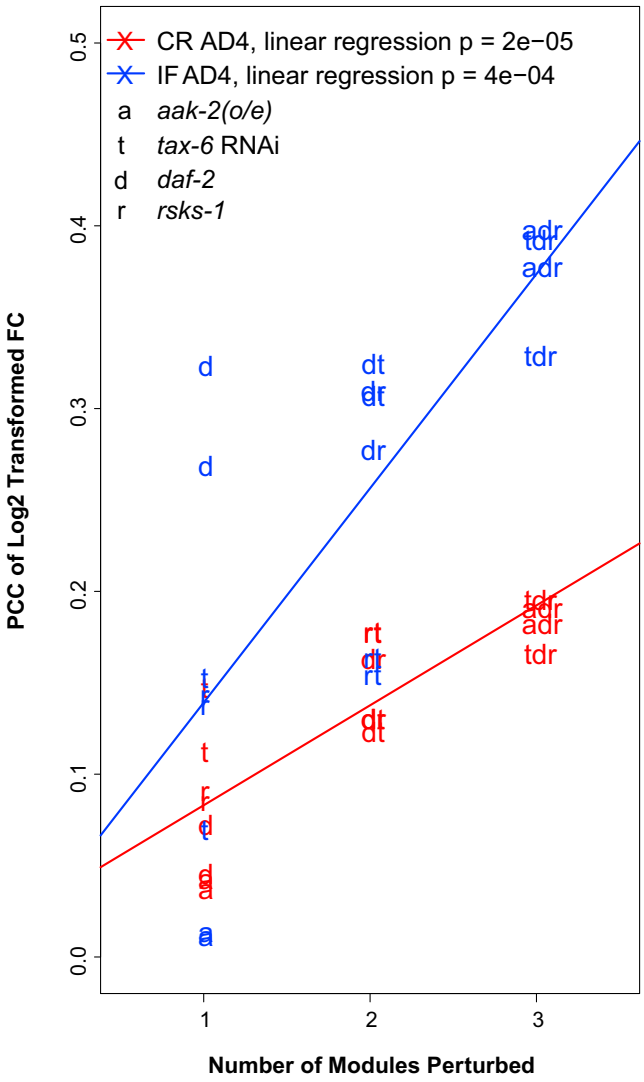

Figure 4. Effect of Simultaneous Perturbation of Three CR/IF-Responding Modules on the Transcriptome

PCC of $\log_2$ fold changes of DR-dependent DEGs between each perturbation condition and CR (in red) or IF condition (in blue) on AD 4. The x axis indicates the number of modules perturbed, while the y axis shows the correlation. Different letters indicate different perturbation samples, and lines show linear regression fits with p values listed on the top of the panel.

See also Figure S3.

two correspond to old states, where prolongevity AAK-2 is fully inactive and one or both of antilongevity DAF-2 and RSKS-1 are fully active (marked by a purple square and triangle, respectively, in Figure 5B as examples).

Based on this distribution, we divided the space for steady states into two zones, "Young" and "Old," and calculated a longevity potential of the network as the proportion of steady states falling to "Young" over the "Old" and "Young" zones combined (Figure 5C, top panel). We then plotted the longevity potential of the network under different perturbations at various perturbation fold changes (Figure 5C bottom panel). Accordant with our microarray results (Figure 4), our model predicts (1) a *daf-2* mutant (represented by "D") could lead to larger lifespan extension than *rsks-1* or *aak-2* single mutants (represented by "R" or "A"); and (2) the triple mutant has higher longevity potential than double mutants, which in turn are higher than single mutants. The first prediction is also consistent with previous studies (Apfeld et al., 2004; Chen et al., 2013) and our observation of the *daf-16_glp-1* module being the last temporally activated module in CR/IF response (Figure 3B), thus indicative of being the most downstream effect on lifespan.

Importantly, the model predicts the triple mutant with weaker perturbations (e.g., 1.5-fold) has higher longevity potential than a single mutant with much stronger perturbations (e.g., 5-fold), implicating a synergistic effect among the three genes/modules (Figure 5C). Such a synergy apparently can be largely attributed to the positive feedback loops as removing them greatly reduced the longevity potential of the triple mutant (Figures S4B and S4C). Furthermore, entropy analysis shows that removing positive feedback loops delays the system phase transition from one state (Old/Young) to the other state (Young/Old) (Figure S4D). Altogether, our dynamic modeling of the network predicts the relative effects of the single, double, and triple mutants on lifespan, and thus revealed that their relative effects and the synergy among the three modules are largely encoded in the network configuration linking the modules. This explains how CR/IF—by moderately perturbing all three of them—can more effectively shift the network states toward longevity than by strongly perturbing any single module in isolation. Indeed, compared to null mutants, the levels of regulators in these three pathways are less perturbed at the transcription level by CR or IF (Figure S4E, t test, $p = 0.0719$).

Simultaneous Perturbation of Three Modules Creates Long-Lived Worms Insensitive to DR

To test the prediction of our models empirically, we assayed lifespan, stress resistance, and motility of the wild-type and various single, double, and triple mutants under both AL and CR conditions. We first examined whether triple perturbations are refractory to DR in terms of health indicators such as heat shock tolerance and motility (Figures S5A and S5B). We found CR improved the heat tolerance for N2 fed with either OP50 or empty vector (EV) containing HT1115 bacteria (log-rank test $p < 0.001$). CR still increased heat tolerance on several single mutants (Figures S5A and S5B). While this CR effect is largely abolished in the *daf-2 rsks-1* double mutant when fed with OP50 bacteria (log-rank test $p > 0.1$, Figure S5A), the double mutant fed with EV-containing bacteria is still responsive to CR-enhanced heat-shock tolerance (log rank test $p < 0.01$, Figure S5B). Meanwhile, both triple perturbations, *aak-2(o/e);daf-2 rsks-1* and *tax-6* RNAi*;daf-2 rsks-1*, rendered worms refractory to CR-induced heat tolerance (log rank test $p > 0.1$; Figures S5A and S5B). Within the time window of AD 10–16, CR treatment significantly enhanced the motility of N2 worms and single perturbations including *aak-2(o/e)*, *rsks-1*, *tax-6* RNAi, and *daf-2* on at least one of the four days monitored, while *daf-2 rsks-1* double mutants and both triple perturbations were insensitive to motility improvement by CR (Figure S5C). Taken together, these data suggest our reverse-engineered triple mutants recapitulate the effects of DR on health-related phenotypes and become refractory to further beneficial effects of DR.

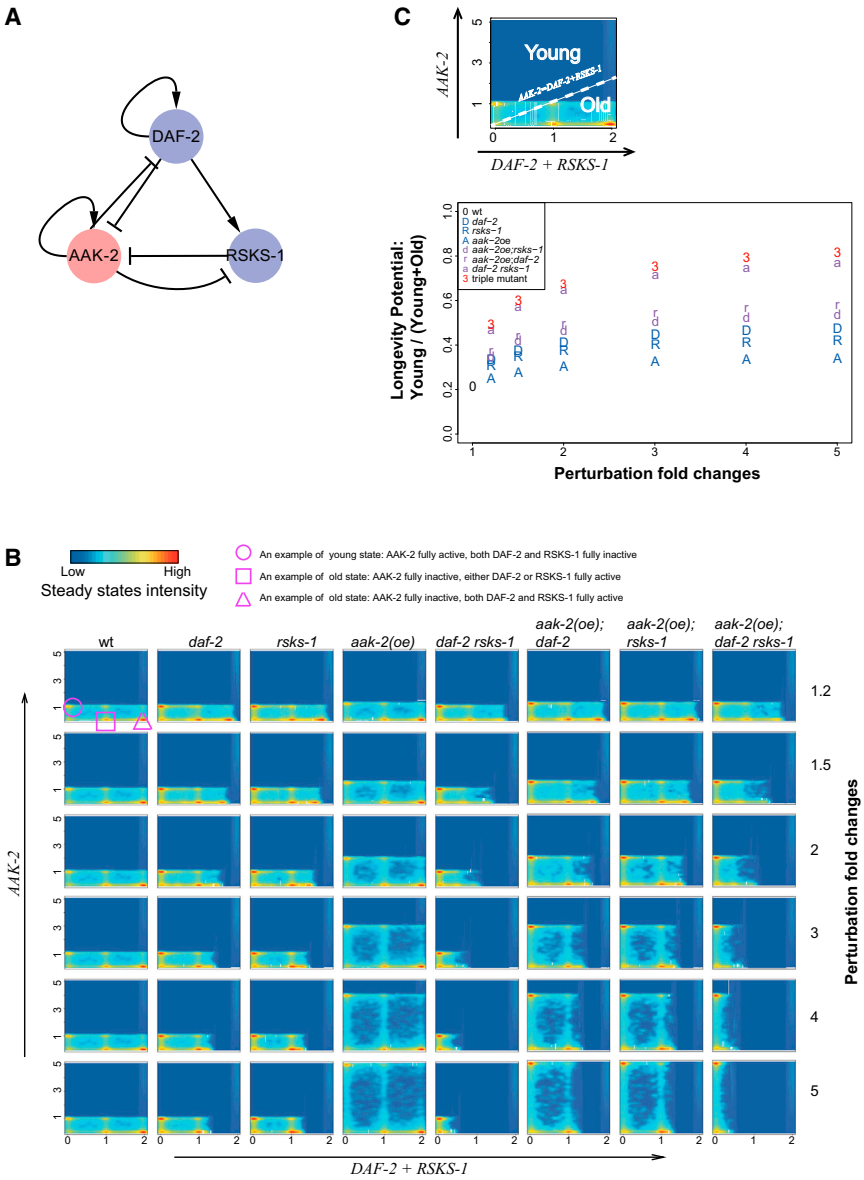

Figure 5. Effect of Simultaneous Perturbation of Three CR/IF-Responding Modules on Network Steady States

(A) DAF-2, RSKS-1, and AAK-2 circuitry derived from literature. Prolongevity and antilongevity factors are labeled pink and purple, respectively. Inhibitory edges are shown with T-shaped arrow; others represent activation.

(B) Distributions of steady states for kinetics of the three factors' circuitry under different perturbation conditions (by column) and different perturbation fold changes (by row). Color intensity from blue to red indicates increasing number of steady states within a parameter space. Purple circle, square, and triangle show examples for each of three types of representative steady states.

(C) Quantification of the simulation results in (B). The y axis shows the proportions of parameter sets giving rise to steady states with *AAK-2* > *DAF-2* + *RSKS-1*, and x axis indicates the fold change of a factor perturbed.

See also Figure S4.

To determine if we could also reverse engineer the longevity effects of DR, we tested the ability of DR to extend lifespan in our triple genetic mutants. As predicted by our regulatory network modularity and the dynamic simulation analyses, when more modules are perturbed the lifespan extension effect of CR diminished—to 63% on N2, 17% on *aak-2(o/e)*, and 19% on *daf-2 rsks-1*—while the triple mutant *aak-2(o/e);daf-2 rsks-1* was completely refractory to lifespan extension caused by CR (log rank test $p > 0.1$) (Figures 6A and S6A; Table S4). These results support our prediction that combined perturbation of the three computationally inferred modules altogether abolishes any further lifespan extension by DR.

We then replaced *aak-2(o/e)* by *tax-6* RNAi to perturb the three modules. We found a clear synergistic effect between *tax-6* RNAi and *daf-2 rsks-1* on lifespan extension (Figures 6B, S6B, and S6C; Table S4) and a total abolishment of CR's lifespan extension effect by the *tax-6* RNAi;*daf-2 rsks-1* triple perturbation (log rank test $p > 0.1$), consistent with the prediction from our dynamic simulation modeling. These *tax-6* experiments not only reconfirmed the requirement of all three modules in DR response but also validated a new role of *tax-6* as a mediator for DR response and demonstrated a superior capability in replacing *aak-2* in the triple pathway manipulation. Unlike *tax-6* RNAi;*daf-2 rsks-1*, which always had longer lifespan than the double mutant under AL conditions in all lifespan assay replicates, *aak-2(o/e)*;*daf-2 rsks-1* did not have longer lifespan than the double mutant (Figures 6A and S6A; Table S4). This suggests that though *aak-2* and *tax-6* act in the same module to synergistically mediate the DR effect—with the *daf-2* and *rsks-1* modules—unlike *tax-6*, *aak-2* may have additional functions not related to DR, which may limit lifespan in the double mutant background (Figures S6D and S6E).

Experimental Validation of Novel Regulators and Interactions Mediating the DR and Longevity Effects

Finally, to further demonstrate the utility of our unbiased systems approach, we tested the effects of the novel predicted lifespan and DR regulators from our BN analysis. In addition to the aforementioned effect of *tax-6* RNAi, we also found that *gas-1* RNAi increases lifespan and was partially refractory to DR (like the other modules) (26.24%, cf. 69.86% increase by DR with EV as control; Figures 7A and S7A and Table S4). As *gas-1* encodes a mitochondrial complex I protein, our BN inference and experimental validation, for the first time, placed its associated mitochondrial function in mediating DR effects.

Although both *aak-2* and *xbp-1* have been known to regulate UPR, whether they act together to modulate aging, as

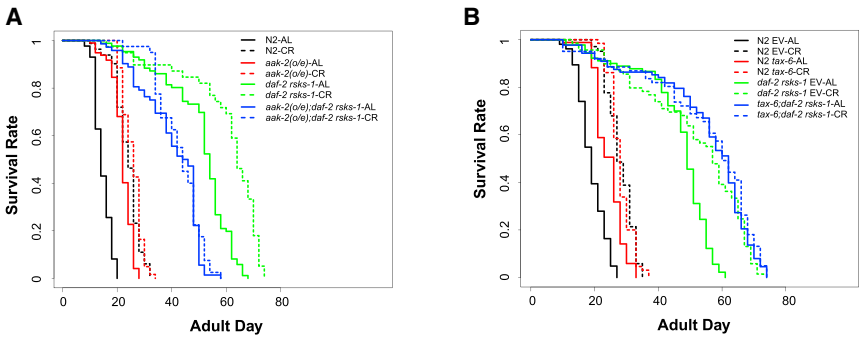

Figure 6. Simultaneous Perturbation of Three Modules Completely Abolished Lifespan Effects of DR

(A) Lifespans of N2, *aak-2 (o/e)*, *daf-2 rsks-1*, and *aak-2 (o/e);daf-2 rsks-1* fed with OP50 bacteria under AL (solid line) or CR condition (dashed line).

(B) Lifespans of N2 and *daf-2 rsks-1* fed with EV or *tax-6* RNAi vector containing bacteria under AL (solid line) or CR condition (dashed line).

See also Figures S5 and S6. Detailed statistics of the lifespan result are presented in Table S4.

suggested by our de novo inference of *aak-2* and *xbp-1* interacting in the same module, was unknown. We tested this hypothesis via epistatic lifespan analysis, and indeed observed that *xbp-1* RNAi repressed lifespan extension by *aak-2(o/e)* (Figures 7B and S7B and Table S4). These results further demonstrate that our systems approach can not only uncover new regulatory circuitry among old players but also brand new regulators in the process of reverse engineering lifespan extension by DR.

DISCUSSION

Here we demonstrate how system approaches can unbiasedly identify novel regulatory networks for DR regimens, which can be synergistically targeted to engineer the full effects of the DR response. We started by mapping temporally resolved *C. elegans* transcriptome changes in response to DR in aging. Intriguingly, in fed wild-type animals we saw an age-dependent reversal of many aging and longevity regulators; in particular, the prolongevity genes are often first upregulated from young to postreproduction age, then decline till death, while the antilongevity genes are exactly the opposite. This is in agreement with the disposal soma theory of aging (Kirkwood, 1977), suggesting that the system has evolved to promote maintenance and suppress DNA damage and cell cycle-related gene expression only during reproduction. Postreproduction, either because the maintenance system is overloaded or because the accumulated DNA damage that has to be dealt with is overwhelming, there is a drastic reversal of the expression trend; gene expression related to DNA damage response keeps increasing and the maintenance genes expression keeps decreasing till death. CR/IF seems to not only delay the transition point but—most importantly—also increases the capacity of the system by further upregulating the maximal level of maintenance gene expression and decreasing the expression of the DNA damage response genes. It would be interesting to see how such system capacity increase is achieved, especially given that *C. elegans* tissues are largely postmitotic.

Based on the three regulatory modules we inferred from the transcriptome changes, we hypothesized that simultaneously perturbing all three modules could recapitulate the full transcriptome changes induced by DR. We validated this prediction by generating double and triple mutants perturbing two or three of the modules. We found that with more modules perturbed the transcriptome changes become more similar to those induced by CR and IF. Despite multiple mechanistic links between different pathways implicated in DR, these data suggest there is no one "master regulator" of the DR response but rather distinct responses targeted by a limited number of distinct perturbations.

To further explore the underlying mechanism of lifespan extension induced by perturbation combinations, we computationally modeled the dynamics of the three-module network and calculated the longevity potential for a perturbation to the nodes and edges of the network based on the probability distribution of steady states after the perturbation. The longevity potential of the perturbations recapitulated increased lifespan extension as more modules are perturbed, and showed a stronger effect of *daf-2* relative to the other two nodes, suggesting these effects are encoded in the network configuration, especially by positive feedback within the network. These data suggest that moderate and simultaneous perturbation of three modules might be even more effective than strong perturbation of each individual module. Despite enlisting all three modules, CR and IF result in smaller lifespan extensions than some genetic perturbations. This is likely due to the fact the DR only moderately, instead of severely perturbed these regulators; indeed, the fold changes of these regulators induced by CR are far less than those from genetic manipulations, such as gene overexpression and inhibition either by RNAi or loss-of-function mutants (Figure S4E). These data suggest that CR/IF increases lifespan through all three modules but that the effect is not maximized, and that stronger perturbation of all three might give greater effects on longevity.

Consistent with this hypothesis, we further demonstrated that by sequentially perturbing more modules, worms progressively became refractory to DR, suggesting our interventions had maxed out the DR effect. We also observed a synergistic effect between *tax-6* RNAi and *daf-2 rsks-1*, as predicted by the modeling. When selecting different prolongevity pathways to generate triple or even quadruple mutants from an engineering perspective, Sagi and Kim have found longer lifespan extension with more pathways perturbed at the same time (Sagi and Kim, 2012), which is indeed genetically expected as long as the pathways can additively or synergistically contribute to longevity. However, a simple knowledge-based engineering approach does not shed light on the underlying mechanism of the combination effect, on whether there is any synergy among different pathways, or in finding new players. Critically, here we use an unbiased systems approach instead of a knowledge-based combinatorial approach. Such a systems approach is tailored to the complex phenotype or system we examined—the DR-induced

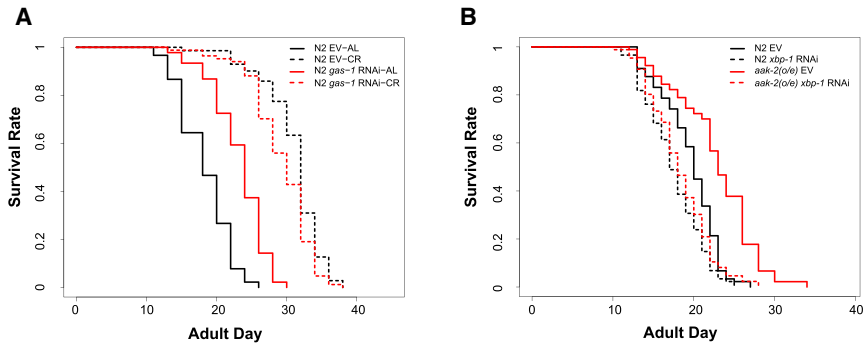

Figure 7. Validation of Novel Regulators and Interactions Mediating DR and Longevity Effects

(A) Lifespans of N2 fed with EV, or *gas-1* RNAi vector containing bacteria under AL (solid line) or CR condition (dashed line).

(B) Lifespans of N2 and *aak-2 (o/e)* fed with EV, or *xbp-1* RNAi vector containing bacteria.

See also Figure S7. Detailed statistics of the lifespan results are presented in Table S4.

transcription and lifespan changes, in this case—and aims to understand the mechanism of the phenotype, rather than simply to maximize lifespan. This therefore represents a paradigm shift from a knowledge-based engineering approach, and one that is critical if we are to utilize the effects of DR in mammals for human therapeutics.

Instead of randomly selecting different pathways, we first identified the full spectrum of modularity of the DR response, inferred modularity regulation, and then utilized the modularity and its regulation to direct synergy on lifespan and DR response and further examined the synergy through network dynamics. In addition, such a systems approach also led to the identification of novel components or regulators of the DR-induced transcription and lifespan changes, such as *gas-1* and *ogt-1*, *tax-6*, and *xbp-1*, and then placed them into well-studied pathways, such as the latter two in the *aak-2* pathway. Among these predictions, we experimentally validated the effect of *tax-6* and *gas-1* on lifespan and DR. Previously there was no evidence for a relationship between *aak-2* and *ire-1/xbp-1* in modulating longevity. With our systems approach, we predicted that *aak-2* and *xbp-1* interacted within the same aging module. This in silico prediction was experimentally validated, since *xbp-1* acts downstream of *aak-2(o/e)* in *C. elegans* longevity. For the first time, these data link AMPK and the UPR in lifespan regulation and illustrate that the power of systems approaches to de novo predict key regulators and interactions for a complex process such as aging and DR.

Theoretically, the modular CR/IF network we uncovered here can be locked in a forever-young state; however, in order for an animal to achieve other functions that maximize its fitness, this may not be the most desirable state. Indeed, it is interesting to note that CR/IF only moderately exploits the system to strike a balance toward longer lifespan, and it would be also interesting to see if other natural processes, such as adult reproduction diapause (Angelo and Van Gilst, 2009), tap into a similar mechanism to achieve a forever-young state. Taken together, our data highlight how no single molecular regulator can recapitulate the full effects of DR. As we aim to translate the conserved mechanism of lifespan extension by DR in model systems to usable therapeutics for human diseases, such a finding is critical. If such a result is conserved in mammals, the most effective method for exploiting DR modulators for disease therapeutics may well require combination approaches that modulate several distinct nodes or modules. A reverse engineering approach, as we used here, is therefore critical if we are to make this goal a reality and translate our knowledge of DR to promote healthy aging.

EXPERIMENTAL PROCEDURES

Detailed methods are described in the Supplemental Information.

Microarray Experiment and Lifespan Analysis

Two batches of microarray were carried out: samples for N2 worms time course microarray experiment were collected according to Figure 1A. AL, CR, and IF treatments were carried out following published protocols (Honjoh et al., 2009), except the concentration of AL was set to 1×10^{10} bacteria/ml while that of CR was set to 1×10^{8} bacteria/ml. Worms with different genetic backgrounds collected on AD 4 were fed with either empty vector (EV) or *tax-6* RNAi vector containing bacteria of AL concentration from hatching. RNA was extracted with Trizol (Invitrogen) and hybridized to Affymetrix GeneChip *C. elegans* Genome Array by CapitalBio Corporation (Beijing, China). The GEO accession number for the microarray expression data above is GSE77111. Other microarray expression data used are listed in Supplemental Information.

Worms were maintained and scored at 20°C. Worms with vulval burst, worm bag, or that were stuck to the plate wall were excluded from lifespan assays.

C. elegans Strains

The *aak-2(o/e);daf-2(e1370) rsks-1(ok1255)* strain was generated and backcrossed six times before being used for lifespan assay together with N2, *aak-2*(o/e) (*uthIs248*[P*aak-2*::*aak-2* genomic (aa1-321)::GFP::*unc54* 3-'UTR, P*myo-2*::tdTOMATO]), *daf-2(e1370) rsks-1(ok1255)*.

Bayesian Network Inference

We collected gene expression fold changes from both our microarray data—CR/IF versus control for each day, and other microarray data—single gene genetic mutant, or RNAi knockdown versus control. Then eDM_BN was used to infer relationships among the dietary and genetic perturbations (comparisons). Afterward, eDM_BN was used to connect inferred regulators/DR mediators and all TFs for which perturbation DEGs or ChIP-seq targets are available, using both real-valued gene expression fold-change data and discretized-valued ChIP-seq TF-target data.

Regulator-Target Network Reconstruction

The regulator-target network (Figure 3C) was inferred in a hierarchical structure with four layers of nodes: DR perturbations, potential mediators of DR, TFs, and gene clusters. (1) Edges among DR perturbations, potential regulators of DR and TFs, are predicted by eDM_BN as described above with default parameters, especially *fc_quantile* = 0.05, *fc_baselevel* = $\log_2(1.5)$, and *fc_width* = 0.6. First-degree neighbors of DR perturbations were taken as DR mediators, as well as two other known DR mediators from the second degree neighbors: AGE-1 and LET-363 (Hansen et al., 2007; Henderson et al., 2006; Honjoh et al., 2009). Only TFs with a direct link to DR mediators are kept. (2) Edges between TFs and clusters were identified through either TF targets or TF DEG (or *xpb-1* mutant and *crh-1* mutant differentially regulated genes, since no ChIP-seq data for these two TFs are available) enrichment

test in each cluster (Fisher's exact test p $\leq$ 1e-5 and the proportions of targets in the cluster $\geq$ 0.1). Only TFs with connection to at least one cluster are kept. (3) Edges between regulators and clusters were identified by cluster genes enrichment test for DEGs upon perturbations (Fisher's exact test p $\leq$ 1e-5 and the proportions of targets in the cluster $\geq$ 0.1). Clusters that connect to no regulator or TF are not included.

Mathematical Modeling for Circuitry Dynamics

The framework proposed by Ma et al. (Ma et al., 2009) is applied here except that we used perturbation factor (PF) instead of 1 for total amount of protein to indicate the perturbation fold changes on a protein. See Supplemental Experimental Procedures for details on assumptions, equations, and simulations.

ACCESSION NUMBERS

The GEO accession number for the microarray expression data above is GSE77111.

SUPPLEMENTAL INFORMATION

Supplemental Information includes seven figures, four tables, and Supplemental Experimental Procedures and can be found with this article at http://dx.doi.org/10.1016/j.cmet.2016.02.002.

AUTHOR CONTRIBUTIONS

J.-D.J.H. and L.H. conceived the study and designed analyses and experiments with suggestions from others. With help from N.S. and D.W., L.H. conducted microarray experiments, network analysis, and simulation. With help from D.C., L.H. and D.W. did lifespan assays, stress tolerance assays, and motility assays. L.Y. developed eDM_BN. Y.Z. and W.M. generated new worm strains and did lifespan assays related to *xbp-1*. H.C. and C.X. collected microarray data for genetic perturbations from the GEO database. J.-D.J.H., L.H., and W.B.M. analyzed the data and wrote the manuscript with help from D.C., D.W., N.S., and J.M.

ACKNOWLEDGMENTS

This work was supported by grants from NSFC 31210103916, 91329302, and 91519330; CAS XDA01010303 and YZ201243; and MOST 2015CB964803 and 2011CB504206 to J.-D.J.H.; from NIH 1R01AG044346 to W.B.M.; from SIBS 2014KIP319 to L.H.; and from NSFC 31371342 to Y.L.

Received: July 21, 2015
Revised: December 14, 2015
Accepted: February 3, 2016
Published: March 8, 2016

REFERENCES

Angelo, G., and Van Gilst, M.R. (2009). Starvation protects germline stem cells and extends reproductive longevity in C. elegans. Science *326*, 954–958.

Apfeld, J., O'Connor, G., McDonagh, T., DiStefano, P.S., and Curtis, R. (2004). The AMP-activated protein kinase AAK-2 links energy levels and insulin-like signals to lifespan in C. elegans. Genes Dev. *18*, 3004–3009.

Baruah, A., Chang, H., Hall, M., Yuan, J., Gordon, S., Johnson, E., Shtessel, L.L., Yee, C., Hekimi, S., Derry, W.B., and Lee, S.S. (2014). CEP-1, the Caenorhabditis elegans p53 homolog, mediates opposing longevity outcomes in mitochondrial electron transport chain mutants. PLoS Genet. *10*, e1004097.

Chen, D., Thomas, E.L., and Kapahi, P. (2009). HIF-1 modulates dietary restriction-mediated lifespan extension via IRE-1 in Caenorhabditis elegans. PLoS Genet. *5*, e1000486.

Chen, D., Li, P.W., Goldstein, B.A., Cai, W., Thomas, E.L., Chen, F., Hubbard, A.E., Melov, S., and Kapahi, P. (2013). Germline signaling mediates the synergistically prolonged longevity produced by double mutations in daf-2 and rsks-1 in *C. elegans*. Cell Rep. *5*, 1600–1610.

Contrino, S., Smith, R.N., Butano, D., Carr, A., Hu, F., Lyne, R., Rutherford, K., Kalderimis, A., Sullivan, J., Carbon, S., et al. (2012). modMine: flexible access to modENCODE data. Nucleic Acids Res. *40*, D1082–D1088.

Crawford, D., Libina, N., and Kenyon, C. (2007). Caenorhabditis elegans integrates food and reproductive signals in lifespan determination. Aging Cell *6*, 715–721.

Fontana, L., Partridge, L., and Longo, V.D. (2010). Extending healthy life span—from yeast to humans. Science *328*, 321–326.

Greer, E.L., and Brunet, A. (2009). Different dietary restriction regimens extend lifespan by both independent and overlapping genetic pathways in C. elegans. Aging Cell *8*, 113–127.

Greer, E.L., Dowlatshahi, D., Banko, M.R., Villen, J., Hoang, K., Blanchard, D., Gygi, S.P., and Brunet, A. (2007). An AMPK-FOXO pathway mediates longevity induced by a novel method of dietary restriction in *C. elegans*. Curr. Biol. *17*, 1646–1656.

Hansen, M., Taubert, S., Crawford, D., Libina, N., Lee, S.J., and Kenyon, C. (2007). Lifespan extension by conditions that inhibit translation in Caenorhabditis elegans. Aging Cell *6*, 95–110.

Henderson, S.T., Bonafè, M., and Johnson, T.E. (2006). daf-16 protects the nematode Caenorhabditis elegans during food deprivation. J. Gerontol. A Biol. Sci. Med. Sci. *61*, 444–460.

Honjoh, S., Yamamoto, T., Uno, M., and Nishida, E. (2009). Signalling through RHEB-1 mediates intermittent fasting-induced longevity in C. elegans. Nature *457*, 726–730.

Kayser, E.B., Sedensky, M.M., and Morgan, P.G. (2004). The effects of complex I function and oxidative damage on lifespan and anesthetic sensitivity in Caenorhabditis elegans. Mech. Ageing Dev. *125*, 455–464.

Kenyon, C.J. (2010). The genetics of ageing. Nature *464*, 504–512.

Kirkwood, T.B. (1977). Evolution of ageing. Nature *270*, 301–304.

Lee, C.K., Klopp, R.G., Weindruch, R., and Prolla, T.A. (1999). Gene expression profile of aging and its retardation by caloric restriction. Science *285*, 1390–1393.

Li, J., Liu, Y., Liu, M., and Han, J.D. (2013). Functional dissection of regulatory models using gene expression data of deletion mutants. PLoS Genet. *9*, e1003757.

Liu, Y., Qiao, N., Zhu, S., Su, M., Sun, N., Boyd-Kirkup, J., and Han, J.D. (2013). A novel Bayesian network inference algorithm for integrative analysis of heterogeneous deep sequencing data. Cell Res. *23*, 440–443.

Ma, W., Trusina, A., El-Samad, H., Lim, W.A., and Tang, C. (2009). Defining network topologies that can achieve biochemical adaptation. Cell *138*, 760–773.

Mair, W., Morantte, I., Rodrigues, A.P., Manning, G., Montminy, M., Shaw, R.J., and Dillin, A. (2011). Lifespan extension induced by AMPK and calcineurin is mediated by CRTC-1 and CREB. Nature *470*, 404–408.

Panowski, S.H., Wolff, S., Aguilaniu, H., Durieux, J., and Dillin, A. (2007). PHA-4/Foxa mediates diet-restriction-induced longevity of C. elegans. Nature *447*, 550–555.

Pletcher, S.D., Macdonald, S.J., Marguerie, R., Certa, U., Stearns, S.C., Goldstein, D.B., and Partridge, L. (2002). Genome-wide transcript profiles in aging and calorically restricted *Drosophila melanogaster*. Curr. Biol. *12*, 712–723.

Qiao, N., Huang, Y., Naveed, H., Green, C.D., and Han, J.D. (2013). CoCiter: an efficient tool to infer gene function by assessing the significance of literature co-citation. PLoS ONE *8*, e74074.

Rahman, M.M., Stuchlick, O., El-Karim, E.G., Stuart, R., Kipreos, E.T., and Wells, L. (2010). Intracellular protein glycosylation modulates insulin mediated lifespan in C. elegans. Aging (Albany, N.Y.) *2*, 678–690.

Sagi, D., and Kim, S.K. (2012). An engineering approach to extending lifespan in C. elegans. PLoS Genet. *8*, e1002780.

Tacutu, R., Craig, T., Budovsky, A., Wuttke, D., Lehmann, G., Taranukha, D., Costa, J., Fraifeld, V.E., and de Magalhães, J.P. (2013). Human Ageing Genomic Resources: integrated databases and tools for the biology and genetics of ageing. Nucleic Acids Res. *41*, D1027–D1033.

Tepper, R.G., Ashraf, J., Kaletsky, R., Kleemann, G., Murphy, C.T., and Bussemaker, H.J. (2013). PQM-1 complements DAF-16 as a key transcriptional regulator of DAF-2-mediated development and longevity. Cell *154*, 676–690.

Uno, M., Honjoh, S., Matsuda, M., Hoshikawa, H., Kishimoto, S., Yamamoto, T., Ebisuya, M., Yamamoto, T., Matsumoto, K., and Nishida, E. (2013). A fasting-responsive signaling pathway that extends life span in *C. elegans*. Cell Rep. *3*, 79–91.

Zhang, W., Liu, Y., Sun, N., Wang, D., Boyd-Kirkup, J., Dou, X., and Han, J.D. (2013). Integrating genomic, epigenomic, and transcriptomic features reveals modular signatures underlying poor prognosis in ovarian cancer. Cell Rep. *4*, 542–553.

Zhou, B., Yang, L., Li, S., Huang, J., Chen, H., Hou, L., Wang, J., Green, C.D., Yan, Z., Huang, X., et al. (2012). Midlife gene expressions identify modulators of aging through dietary interventions. Proc. Natl. Acad. Sci. USA *109*, E1201–E1209.